Biosensors and Bioelectronics 131 (2019) 37–45

Contents lists available at ScienceDirect

Biosensors and Bioelectronics

journal homepage: www.elsevier.com/locate/bios

Flexible, multifunctional neural probe with liquid metal enabled, ultra-large tunable stiffness for deep-brain chemical sensing and agent delivery

Ximiao Wen[a,1], Bo Wang[b,1], Shan Huang[c], Tingyi "Leo" Liu[d], Meng-Shiue Lee[e], Pei-Shan Chung[f], Yu Ting Chow[a], I-Wen Huang[g], Harold G. Monbouquette[g], Nigel T. Maidment[b,*], Pei-Yu Chiou[a,f,*]

[a] Department of Mechanical and Aerospace Engineering, University of California at Los Angeles, Los Angeles, CA, USA
[b] Department of Psychiatry & Biobehavioral Sciences, Semel Institute for Neuroscience and Human Behavior, University of California at Los Angeles, CA, USA
[c] Department of Biological Chemistry, University of California at Los Angeles, CA, USA
[d] Department of Mechanical and Industrial Engineering, University of Massachusetts Amherst, MA, USA
[e] Department of Mechanical Engineering, National Chiao Tung University, Hsinchu, Taiwan
[f] Department of Bioengineering, University of California at Los Angeles, CA, USA
[g] Department of Chemical and Biomolecular Engineering, University of California at Los Angeles, CA, USA

ARTICLE INFO

Keywords:
Neural probes
Electrochemical biosensors
Drug delivery
Liquid metal
Flexible electronics

ABSTRACT

Flexible neural probes have been pursued previously to minimize the mechanical mismatch between soft neural tissues and implants and thereby improve long-term performance. However, difficulties with insertion of such probes deep into the brain severely restricts their utility. We describe a solution to this problem using gallium (Ga) in probe construction, taking advantage of the solid-to-liquid phase change of the metal at body temperature and probe shape deformation to provide temperature-dependent control of stiffness over 5 orders of magnitude. Probes in the stiff state were successfully inserted 2 cm-deep into agarose gel "brain phantoms" and into rat brains under cooled conditions where, upon Ga melting, they became ultra soft, flexible, and stretchable in all directions. The current 30 μm-thick probes incorporated multilayer, deformable microfluidic channels for chemical agent delivery, electrical interconnects through Ga wires, and high-performance electrochemical glutamate sensing. These PDMS-based microprobes of ultra-large tunable stiffness (ULTS) should serve as an attractive platform for multifunctional chronic neural implants.

1. Introduction

Implantable neural probes constitute an important class of technologies used by neuroscientists both to modulate and to detect electrical and chemical neuronal activities in the brain. These tools are also employed clinically for deep brain stimulation (DBS), a treatment for several conditions, including Parkinson's disease, epilepsy, depression and obsessive compulsive disorder (OCD) (Minev et al., 2015; Park et al., 2016; Rivnay et al., 2017). For research purposes, neural probes are often implanted in assemblies with injection cannulae for local microinjection of drugs or viruses thereby providing an additional level of neurological manipulation and control (Jeong et al., 2015a; Rohatgi et al., 2009). However, such assemblies can cause significant damage to the targeted brain region due to their large footprint (Sim et al., 2017). In the past ~30 years, the development of microelectromechanical systems (MEMS) has led to the creation of silicon-based neural probes with integrated microfluidic channels for material delivery (Chen et al., 1997; McAllister et al., 2003; Reed and Lye, 2004). While smaller overall, the large mechanical mismatch and micromotion between such rigid probes (E = 200 GPa) and soft brain tissue (E = 0.4–15 kPa) is one of several possible triggers of the long-term inflammatory responses that cause neuronal loss and scar formation around the implants, limiting their chronic recording and stimulating capabilities (Jeong et al., 2015b; Jorfi et al., 2015; Rivnay et al., 2017).

In recent years, flexible probes based on plastics such as polyimide and SU-8 have been developed in an attempt to circumvent the mechanical mismatch problem by shrinking the probe dimension aggressively to micron-scale (Liu et al., 2015; Luan et al., 2017; Wu et al., 2015). However, the desirably weak mechanical stiffness presents a major challenge during the deep-brain implantation process. To mitigate this issue, soft probes were either coated with stiffening polymer that dissolves after implantation (Tien et al., 2013; Xiang et al., 2014),

* Correspondence to: University of California Los Angeles, CA 90095, USA.
E-mail addresses: nmaidmen@g.ucla.edu (N.T. Maidment), pychiou@seas.ucla.edu (P.-Y. Chiou).
[1] These authors contributed equally to this work.

https://doi.org/10.1016/j.bios.2019.01.060
Received 6 November 2018; Received in revised form 21 January 2019; Accepted 24 January 2019
Available online 07 February 2019
0956-5663/

or were made of polymers that soften after implantation (Capadona et al., 2012; Ware et al., 2014). However, deep-brain implantation (> 3 mm) is challenging for such probes due to the low Young's modulus (~2 GPa) of such polymers resulting in the need for large cross-sectional areas to provide sufficient stiffness to prevent buckling during insertion (Tien et al., 2013; Weltman et al., 2016; Wu et al., 2015; Xiang et al., 2014). Soft probes can also be attached to a stiff shuttle, such as a metal syringe or a silicon probe, that can be retracted after insertion (Liu et al., 2015; Luan et al., 2017; Kim et al., 2013). However, the final location of the inserted probes may be disturbed during shuttle retraction and the shuttle may cause undesirable tissue damage (Felix et al., 2013). These latter approaches also require a labor intensive high-precision manual alignment and assembly process, particularly when multi-shank and 3D probe arrays are desired for multi-region recording. Another major concern of some prior flexible probes, such as injectable mesh electrodes or super thin plastic films, is that the materials used in such probes are still “hard” (plastics and nanowires). Thus, the probe structures need to be extremely thin and narrow in order to be flexible, which may compromise the functions that can be integrated on a probe. For example, integration of fluid channels on these probes for drug delivery is difficult since the flow resistance in a channel increases inversely with thickness by ($1/t^3$) (Bruus, 2011). Sensitivity of integrated electrochemical sensing electrodes on these narrow probe structures may also be compromised by their necessarily small surface area. The above-mentioned functions enable the monitoring of chemical transmission and manipulation of brain activities, which are extremely important in understanding brain functions and dissection of neural circuits.

To solve these confounding issues encountered by current flexible probes, here, we present a multifunctional, flexible and stretchable neural probe for chemical sensing and chemical delivery. The stiffness of this probe can be tuned by 5 orders of magnitude before and after brain insertion, thereby enabling self-implantation into deep brain regions without using external shuttle carriers. Once implanted, the probe becomes soft and flexible within a few minutes. With miniaturized design (30 μm-thick) and soft substrate material (E~1 MPa), this flexible and stretchable probe causes less tissue damage induced by brain movements in all directions (Nguyen et al., 2014; Subbaroyan et al., 2005). Deposition of appropriate enzymes and exclusion polymers onto platinum (Pt) microelectrode sites on the probe permits high-sensitivity electrochemical detection of neurotransmitters in deep-lying brain structures, and the integration of microfluidic channels allows delivery of drugs and other chemicals in the local vicinity of the sensing sites.

2. Experimental section

2.1. ULTS probe design and working principle

The multifunctional, ultra-large tunable stiffness (ULTS) probe is a compact, multi-layer, free-standing structure that integrates Pt electrodes, microfluidic channels, and electrical interconnects, all on a 30 μm-thick PDMS structure (Fig. 1a). PDMS was used as the structural material due to its low Young's Modulus (E~1 MPa), high stretchability, and biocompatibility (Lee et al., 2016; Minev et al., 2015). Pt microelectrodes for high sensitivity electrochemical sensing were fabricated on small, thin silicon dioxide islands on a separate silicon substrate and transferred onto the ULTS probe. To provide electrical connections to these electrodes on the flexible and stretchable probe without cracking and delamination issues, gallium (Ga), a liquid metal, was used due to its fluidity, high electrical conductivity, and biocompatability (Chow et al., 2018; Dickey, 2017; Hallfors et al., 2013).

Two key physical material properties—the elasticity of PDMS (Fig. 1b) and the near-body-temperature melting point of Ga (~30 °C)—were needed to realize the large tunable stiffness property of our probes. During fabrication, pressurized liquid Ga was introduced into the stretchable microfluidic “stiffening” channel to deform and enlarge the cross section of the probe and then frozen to solid state (E = 10 GPa) to achieve a stiff probe for deep brain implantation (Fig. 1c). At body temperature (~37 °C), Ga melted and was removed from the stiffening channel by suction to reduce probe thickness and stiffness (Fig. 1d). During probe implantation, the brain tissue was transiently cooled to below 30 °C by application of chilled saline to the skull surface, a commonly used local and reversible experimental neuronal inhibition method (Long and Fee, 2008; Peel et al., 2017) and therapeutic process for neuroprotection (Dietrich et al., 2009; Kuluz et al., 1992). After implantation, Ga melted immediately upon brain temperature recovery (Fig. 1e–g).

2.2. Fabrication of ULTS probes

The multifunctional ULTS probes were fabricated on silicon wafers using conventional microfabrication processes for electrode patterning, and a customized PDMS thin-film transfer process to form the probe substrate and microchannels with 1 drug delivery port and 2 electrochemical sensing sites. Detailed steps involved in the fabrication of ULTS probes are illustrated in Supplementary Fig. S1, and details of the PDMS thin-film transfer process are described in Supplementary Fig. S2. Key fabrication processes are summarized as follow: (i) Pt electrodes, soldering pads and SiO_2 insulators were patterned on a silicon substrate, which serves as a sacrificial layer. (ii) PDMS thin-film was deposited and patterned by a PDMS lift-off process. This layer of PDMS physically connects the electrodes on the probe tip with the probe base, as well as providing bottom passivation of electrical interconnects and drug delivery channel. (iii) A second PDMS thin-film with microfluidic channels and top passivation was transferred and bonded to the first PDMS layer *via* O_2 plasma (80 W, 500 mT, 30 s). (iv) A third PDMS stiffening channel was transferred and bonded *via* O_2 plasma. (v) Liquid Ga was injected into interconnects and stiffening channels and frozen to solid state to maintain the shape and strength after XeF_2 releasing process. (vi) The probes were released by the silicon undercut using XeF_2. A 2 cm-long single-shank ULTS probe and a 1 cm-long 4-shank probe are designed to demonstrate the mechanical properties of ULTS probes.

Similar to our prior silicon-based probes (Wang et al., 2018), the oval-shaped sensing electrodes (40 × 150 μm, width × length) are located at the tip of the probe shank (0.144 × 9 mm, width × length). Key dimensions of the three PDMS layers and associated channels are as follows: bottom substrate, 5 μm thick, wire & drug delivery channel, 10 μm thick, stiffening channel, 15 μm thick, microchannels for electrical interconnects and drug delivery, 15 × 5 μm (width × height), Ga stiffening channel, 104 × 10 μm (width × height). These conservative design parameters were chosen to achieve a high fabrication yield and may be modified in the future to further reduce the probe dimensions.

2.3. Biosensor preparation

Pt microelectrodes on the ULTS probes were modified to serve as enzymatic biosensors for detection of glutamate (Glut), the major excitatory neurotransmitter in the mammalian central nervous system (Danbolt, 2001; Gass and Foster Olive, 2008). Amperometric electroenzymatic methods for the near real-time detection of Glut and other neurochemicals have been described previously using Pt microelectrodes coated with crosslinked, H_2O_2-generating oxidases (*e.g.* glutamate oxidase (GlutOx)) (Tolosa et al., 2013; Wassum et al., 2008).H_2O_2, generated from the oxidation of substrate (*i.e.,* analyte), which is catalyzed by the oxidase, is electrooxidized by the application of anodic potential to the underlying Pt microelectrodes. The resultant electrical current signals are recorded and correlated to analyte concentration. A layer of poly-m-phenylenediamine (PPD) was electrodeposited on the Pt microelectrodes in this study to block the common electroactive interferents in the rat striatum, dopamine (DA) and ascorbic acid (AA) (Wahono et al., 2012; Wang et al., 2018).

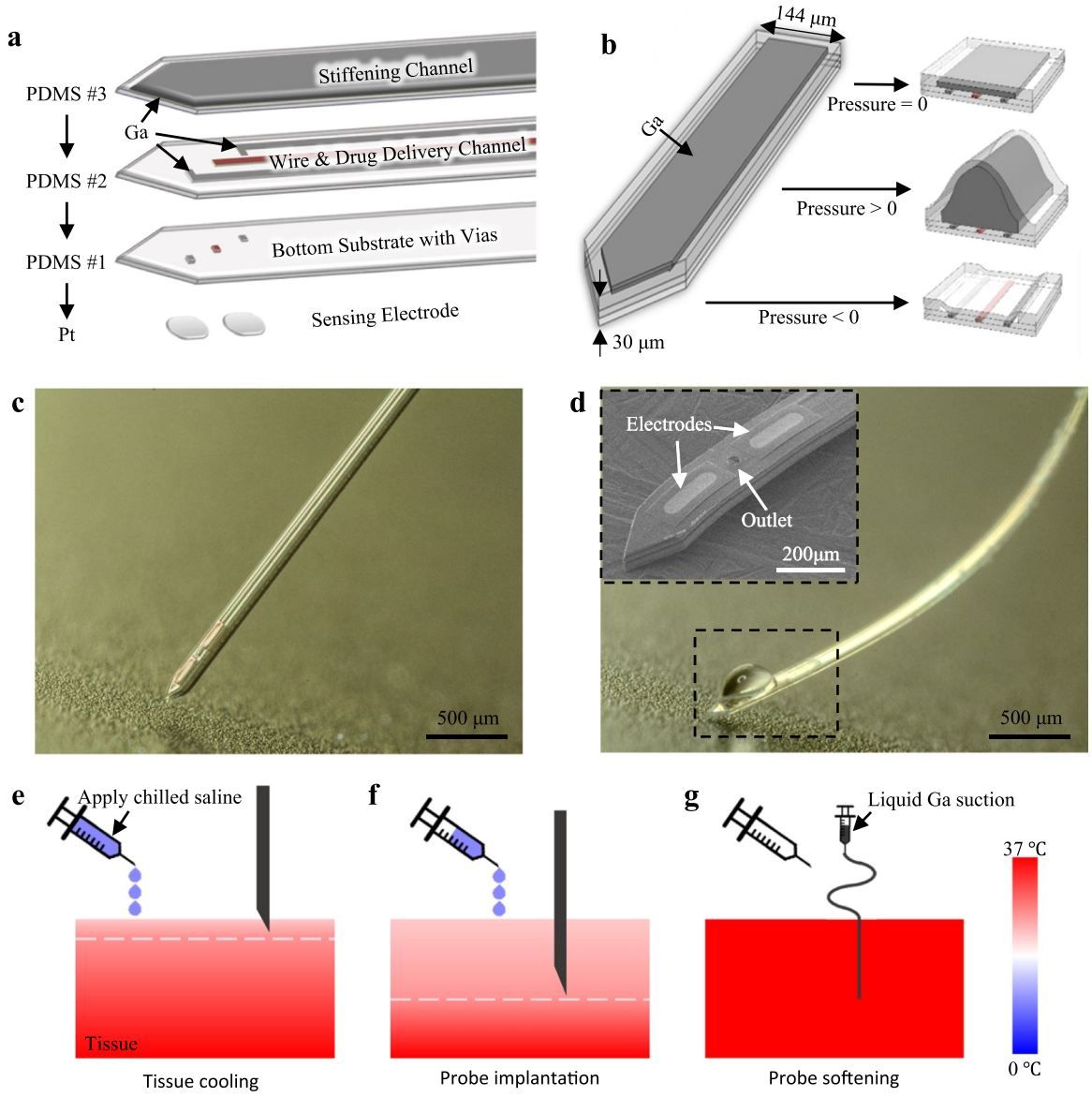

Fig. 1. Design and working principle of ULTS probes. (**a**) An exploded-view drawing of a ULTS probe with 3 layers of PDMS thin-films integrated with Pt electrodes for electrochemical sensing. The first PDMS layer serves as the bottom substrate of the probe. Three through-layer holes (vias) are patterned, one serving as liquid outlet, and two for electrical connection to the sensing electrodes. The second PDMS layer is composed of three microfluidic channels, one for drug delivery and two filled with liquid metal (Ga) for electrical connections. The third PDMS layer has one liquid channel filled with liquid Ga, which is then frozen to stiffen the probe. (**b**) Schematics illustrating the swelling of the ULTS probe shank under different Ga filling pressures: i) no pressure, flat state; ii) positive pressure, inflated state; iii) negative pressure (suction), deflated state. (**c**) Picture of a fabricated ULTS probe in the stiff state for brain implantation. (**d**) A ULTS probe in the soft state with integrated drug delivery function. Inset, a SEM image of the probe tip showing the outlet of the drug delivery channel and Pt electrodes. (**e–g**) Schematic of the implantation procedure. Tissue is cooled down from the surface by the application of chilled saline. The white dashed line represents the temperature of the Ga melting point, 30 °C, above which the probe becomes flexible. After implantation, Ga melts and is removed from the stiffening channel by suction to reduce probe thickness and stiffness. Temperature is represented in color scale.

All electrochemical experiments were conducted inside Faraday cages, and experimental setups are summarized in Supplementary Fig. S3. Electrochemical preparation and characterization of the microelectrode sensors were performed using a Versatile Multichannel Potentiostat (model VMP3) equipped with the 'p' low current option and low current 'N' stat box (Bio-Logic USA, LLC, Knoxville, TN, USA) in a three-electrode configuration.

For sensor preparation, microelectrodes on ULTS probes were rinsed with DI water followed by an electrochemical cleaning step with 0.5 M sulfuric acid. Electropolymerization of m-phenylenediamine on the electrode surface was conducted using a Pt wire counter electrode, a glass encased Ag/AgCl in 3 M NaCl solution reference electrode (Bioanalytical Systems, Inc., West Lafayette, IN, USA) (Supplementary Fig. S3a), and a Pt working electrode on the ULTS probe immersed in a stirred solution of 5 mM m-phenylenediamine in phosphate-buffered saline (PBS), with an applied potential of 0.85 V *vs.* Ag/AgCl for 15 min. After PPD deposition, the GlutOx solution for enzyme immobilization was prepared by mixing 2 μL GlutOx (250 unit/mL) with 3 μL BSA solution (10 mg/mL) containing glutaraldehyde (0.125% v/v). A ~0.1 mL drop of the solution was formed on a syringe tip and gently swiped across the microelectrode sites at the probe tip. This procedure was repeated 11 times for optimal sensitivity (Wassum et al., 2012). The resulting Glut sensor microprobe was left to dry overnight in a desiccator at 4 °C.

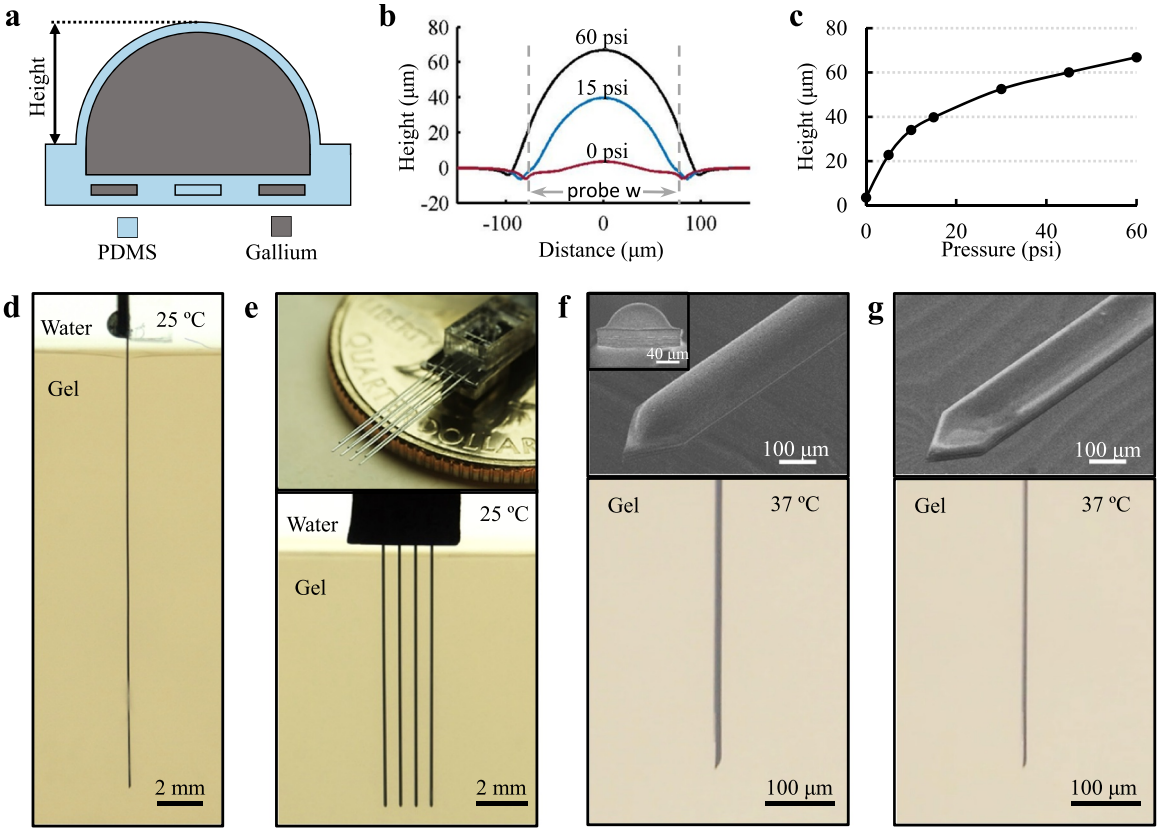

Fig. 2. Characterization of probe tunable stiffness and implantation capability in brain phantoms. (**a**) Schematic cross-sectional view of an inflated probe. (**b,c**) Characterization of the probe shank swelling with respect to different Ga filling pressure. Dashed lines represent the boundaries of the probe (144 μm-wide). The slightly longer distance under 60 psi is a measurement artifact due to steep edge of the largely deformed probe and the cone shape of the profilometer's stylus. (**d**) Demonstration of a 2 cm-long ULTS probe implanted in a brain phantom (0.6% agarose gel) at room temperature, with a Ga injection pressure of 60 psi to achieve maximum stiffness. (**e**) Top, picture of a 4 × 2 probe array by stacking two 4-shank probes. Bottom, insertion of a 1 cm-long, 4-shank probe in a brain phantom. (**f**) ULTS probe in the "inflated" state with 15 psi injection pressure. Top, SEM 'bird's-eye' view. Inset, front view showing a shank swelling height of 40 μm, scale bar, 40 μm. Bottom, side-view of an inflated probe implanted in a brain phantom. (**g**) ULTS probe in the "deflated" state. Top, SEM 'bird's eye' view. Bottom, side-view of a probe in a brain phantom deflated by active suction of Ga.

2.4. In vitro biosensor characterization and testing

A separate microscale iridium oxide (IrOx) reference electrode, described previously (Tolosa et al., 2013) was used for *in vitro* and *in vivo* experiments (Supplementary Fig. S3b). Before IrOx deposition, electrode surfaces were first modified with Pt nanoparticles to increase the surface area (Boehler et al., 2015). To characterize the biosensor, a potential of 0.6 V was applied *vs.* IrOx in a beaker containing 10 mL of stirred PBS solution, and three 20 μL aliquots of Glut (10 mM) were consecutively added to the same beaker to reach final Glut concentrations of 20, 40 and 60 μM. Additionally, aliquots of the potential interferents, AA and DA, were added to the beaker to attain physiological brain concentrations of 250 μM and 5–10 μM, respectively, to confirm selectivity for Glut over the interferents at physiological concentrations (Spector, 1977; Eriksson et al., 1999). To characterize the linear range of the biosensor, eight 20 μL aliquots of Glut (10 mM) were sequentially added to the beaker containing 10 mL PBS solution to reach final Glut concentrations of 20, 40, 60, 80, 100, 120, 140 and 160 μM. Before making measurements, 30 min of equilibrium time immersed in PBS was required for the current detected to approach a constant baseline.

Electrochemical sensing experiments in brain phantoms (0.6% agarose gel in artificial cerebrospinal fluid (aCSF)) were conducted with a multichannel FAST-16 potentiostat (Quanteon, LLC, Lexington, KY, USA) using a two-electrode system consisting of a separate microscale IrOx reference electrode and Glut biosensors on the ULTS microprobe (Supplementary Fig. S3d). Amperometric data were collected at 80 kHz, averaged over 0.1 s intervals and further processed using a moving average filter with 11 input points in MATLAB to remove noise at 1 Hz.

2.5. Acute in vivo studies

Each Glut biosensor on the ULTS microprobe was calibrated (sensitivity and selectivity) right before and after the *in vivo* studies (Supplementary Fig. S3c). A calibration factor based on analysis of these data was calculated for each electrode on the ULTS microprobes to be used for *in vivo* experiments. *In vivo* electrochemical sensing experiments were conducted in the same configuration as in brain phantoms (Supplementary Fig. S3d), except for a longer equilibrium time of 60 min.

Male Sprague Dawley rats (260–330 g) were anesthetized with isoflurane and placed in a standard stereotaxic frame for surgery. All experimental procedures and surgeries were conducted in accordance with the Institutional Animal Care and Use Committee of UCLA.

A microscale temperature probe (HYP1-30-1/2-T-G-60-SMP-M, Omega Engineering, Inc.) was lowered through a craniotomy to a depth of 5.0 mm at a site remote from the recording area. Chilled sterile saline (~10 °C) was perfused across the skull surface at a flow rate of 1–3 mL/min to cool the brain tissue to just below 30 °C. The pre-calibrated ULTS probe was then unilaterally implanted into the right striatum (from bregma: A/P + 1.0 mm, M/L +2.5 mm and D/V −5.0 mm) according to the atlas of Paxinos and Watson (4th ed.). After insertion of the probe, the temperature probe was removed and replaced by a microscale IrOx reference electrode at the same location. Animals remained under anesthesia throughout the experiment. High potassium (100 mM)

artificial cerebrospinal fluid (aCSF: 27.5 mM NaCl, 100 mM KCl, 0.9 mM NaH_2PO_4, 5 mM Na_2HPO_4, 1.2 mM $CaCl_2$, 1 mM $MgCl_2$, pH 7.4) or Glut (500 μM in normal aCSF–as above except 125 mM NaCl and 2.5 mM KCl) was injected when the electrode signal reached the equilibrium state.

Changes in signals were recorded following pressure injection of high potassium aCSF or Glut by a pressure source (FemtoJet, Eppendorf) at various time intervals. Responses were recorded across a range of signal amplitudes by increasing the duration of pressure injection (0.3–4.8 s) and thereby increasing the volume injected (~1–20 nL).

3. Results and discussion

3.1. Characterization of probe tunable stiffness and implantation in brain phantoms

To investigate the tunable stiffness range, we first characterized the probe deformation with respect to different Ga filling pressures using a contact profilometer (Fig. 2a–c). The maximum pressure injected was 60 psi, which resulted in the largest channel deformation of ~67 μm. The range of tunable bending stiffness was determined based on the Young's modulus and the probe shape between the “stiff”, inflated state and the “soft”, deflated state. For estimation, the expanded shape was approximated to be a semi-circle (profile at 30 psi) with a radius of 52 μm. This resulted in a stiffness difference of 5 orders of magnitude between these two states, where the Ga phase change contributes ~4 orders of magnitude and the shape change contributes the remaining 10-fold difference (Supplementary Fig. S4). A larger tunable range can be obtained if using softer elastomers with higher stretchability, which can further increase its softness in the “soft” state as well as its stiffness in the “stiff” state due to the larger deformation under the same filling pressure.

We implanted the ULTS probes in brain phantoms (0.6% agarose gel), which has similar mechanical properties to neural tissue (Jeong et al., 2015a). A 2 cm-long ULTS probe, filled with Ga at 60 psi, could be implanted successfully into this brain phantom in “stiff” state at room temperature (Fig. 2d), whereas a probe in “soft” state at elevated temperature ($T > 30\,^{\circ}C$) deformed upon contact with the brain phantom surface. A four-shank ULTS probe was also fabricated and implanted successfully into the brain phantom, demonstrating the capability to scale up to multi-shank probes for large volume neural recordings (Fig. 2e). After implantation, the brain phantom was heated in a water bath to 37 °C to simulate brain temperature recovery. Ga melted and the stiffening channel was deflated by active suction from the inlet of the Ga channel to reduce the bending stiffness in the “soft” state (Fig. 2f, g).

3.2. Demonstration of probe flexibility in brain phantoms

To demonstrate the flexibility of ULTS probes, we moved the probe/brain phantoms to simulate the relative motion between the brain and the skull. As shown in Fig. 3a, the implanted portion of our flexible probe remained steady regardless of the probe movement above the brain phantom. We also compared ULTS probes with silicon and SU-8 based probes of similar dimension, which created large “wounds” (Fig. 3b-e and Supplementary Movie 1). The experiment demonstrated significant reduction of relative motion in all directions compared to probes made of stiffer materials as suggested from previous simulations (Subbaroyan et al., 2005).

3.3. In vitro probe characterization

Fig. 4a. illustrates the structure of a biosensor. The sensitivity (8.2 ± 1.2 pA/μM), detection limit (0.39 ± 0.07 μM at a signal-to-noise ratio of 3; n = 4) and response time (~1 s) achieved are comparable to the performance characteristics of our prior silicon-based microprobes with the same sensor design (Tolosa et al., 2013; Wassum et al., 2008). With repetitive addition of Glut, the sensors displayed a linear response up to 160 μM ($R^2 = 0.994$) (Fig. 4b and Supplementary Fig. S5a), which covers the physiological range (Tolosa et al., 2013; Wassum et al., 2008). For the same sensors, AA and DA were successfully excluded at supra-physiological concentrations by the PPD layer (Fig. 4c).

The drug delivery function of the ULTS probes was initially evaluated by using a pressure source to inject an aqueous solution of Allura Red AC from the probe into brain phantom (Fig. 4d). The flow rate through the PDMS microfluidic channel was linear with pumping pressures in the range of 30–60 psi ($R^2 = 0.995$; n = 3) (Supplementary Fig. S5b). Local injections of H_2O_2 (40 μM) and Glut (150 μM) *via* the channel into brain phantoms (0.6% agarose gel in aCSF), were rapidly detected by the biosensors, the signal amplitude varying with injection volume (Fig. 4e, f).

For the current probes, the number of microelectrodes was limited by the large microelectrode size required by electrochemical sensing rather than by the number of electrical interconnects. In contrast, the linewidth of microchannels is defined by lithography, meaning they can be potentially scaled to match the microelectrode count of conventional MEA probes. Although electrophysiological recording and electrical stimulation were not performed in this study, the impedance of the electrodes, 21.4 ± 1.50 kΩ (n = 5) at 1 kHz (Supplementary Fig. S6a), is identical to silicon-based probes with Pt electrodes due to the highly conductive liquid metal interconnects. Moreover, a rough Pt surface (Pt grass) (Boehler et al., 2015) can be deposited electrochemically to increase the effective surface area and lower the impedance to 6.74 ± 0.49 kΩ (n = 3) at 1 kHz (Supplementary Fig. S6b) resulting in a charge storage capacity of 4.5 mC/cm^2 (Supplementary Fig. S6c). Therefore, with modified electrode design, ULTS probes can be readily adapted for electrophysiological recording and electrical stimulation applications.

3.4. Probe implantation in rats

We implanted probes in the striatum of rats (Fig. 5a) under continuous isoflurane anesthesia to test their performance *in vivo*. In a typical implantation procedure (Fig. 5b), a 30-gauge mini hypodermic temperature probe was implanted remote from the recording area to monitor the brain temperature at the target implantation depth of the ULTS probe. Chilled sterile saline (~10 °C) was then perfused over the exposed skull surface to reduce the brain temperature to approximately 28 °C at the targeted depth thereby ensuring that the probe would remain straight and stiff throughout the entire implantation procedure. The ULTS probe was then stereotaxically lowered to the targeted region over approximately one minute (Fig. 5c). The body temperature of the rats was kept at 37 °C by a heating pad. The cooling process typically lasted < 10 min, and the brain temperature recovered to baseline in a few minutes (Fig. 5d). We confirmed probe localization within the striatum by bright-field microscopy of brain sections post-mortem (Supplementary Fig. S7).

Implantation of ULTS probes requires selective brain cooling, without altering the core temperature. This practice has been widely used to locally and reversibly inhibit neural activity and alter behavior in research settings, as well as clinically, *e.g.* for treatment of hypoxic ischemic neonatal encephalopathy, stroke and brain trauma (Wang et al., 2014). As shown repeatedly, brain tissue tolerates well significant temperature reduction for brief periods (1–3 h) (Galuske et al., 2002; Girard and Bullier, 1989; Oku et al., 2009; Percy et al., 2009).

3.5. In vivo probe testing

Electrochemical sensing and drug delivery functions of the ULTS probe were evaluated under continuous anesthesia. Glut (500 μM in

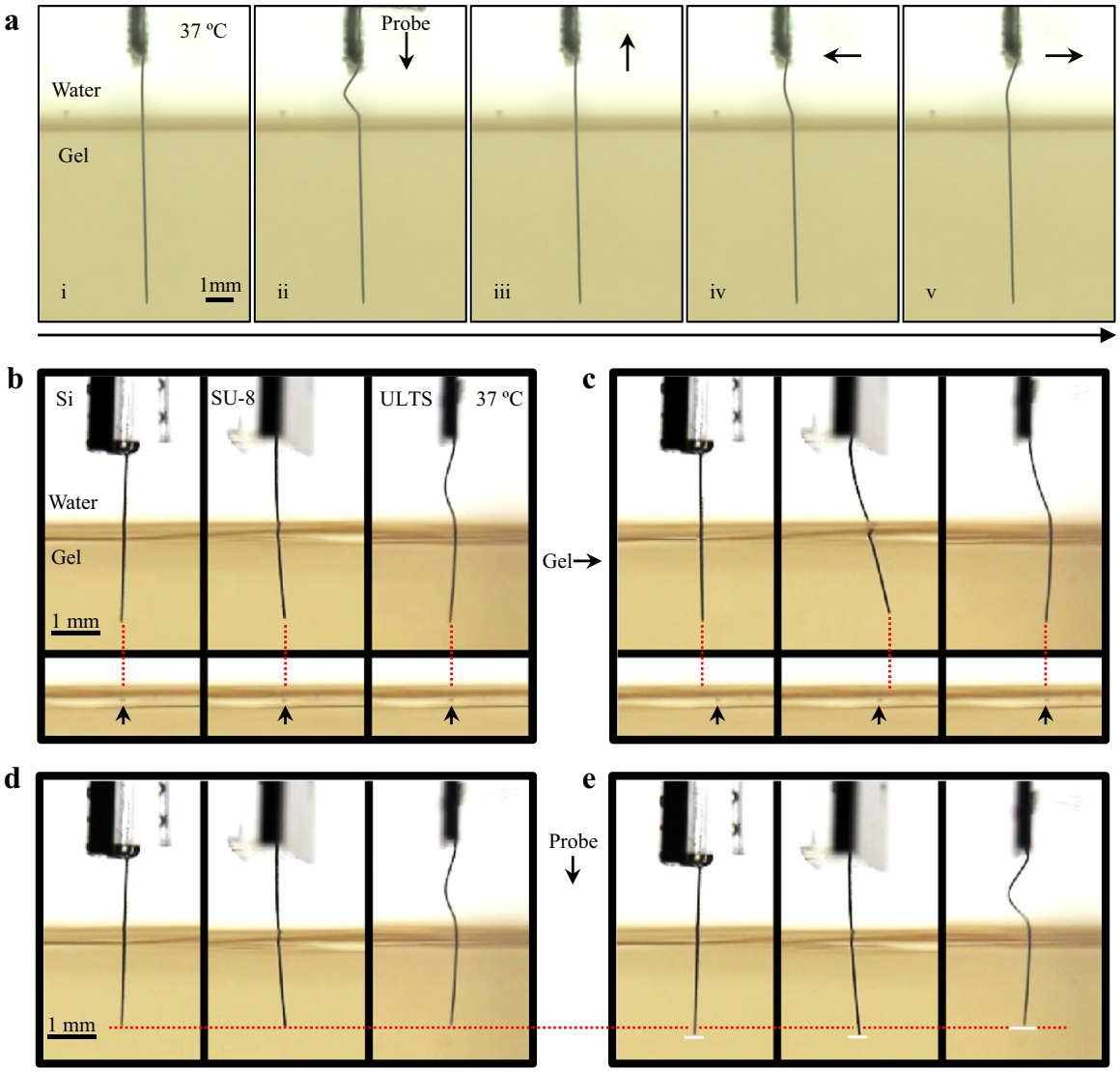

Fig. 3. Demonstration of probe flexibility in brain phantoms. (**a**) Pictures of a "soft" ULTS probe in a brain phantom. Probe base was moved in all directions to simulate the relative motion between skull and brain with no resulting deformation of the brain phantom. (**b,c**) Comparison of silicon (Si), SU-8 and ULTS probes with a 500 μm horizontal movement of the brain phantom. Each dotted line is extended from the probe tip vertically. Arrows indicate the reference points in the brain phantom. (**d,e**) Comparison of Si, SU-8 and ULTS probes with a vertical movement of the probe base. The dotted line indicates the original level of probe tips. Solid lines in (e) indicate the probe tips' positions after probe movement.

aCSF) was pressure-ejected using varying pressure pulse durations to control injection volumes (Fig. 6a). The signal evoked at the sensors by Glut ejection was highly reproducible and typically returned to baseline within 5 s of pressure pulse termination, compared to approximately 100 s in brain phantoms, reflecting differences in diffusion and the presence of active reuptake in brain tissue (Supplementary Fig. S8). Endogenous Glut release was evoked by repeated local ejections of potassium-enriched artificial cerebrospinal fluid (100 mM K^+ aCSF) (Fig. 6b). As we reported previously using silicon-based MEA/injection cannula assemblies (Walker et al., 2007), signal amplitude declined abruptly after the first of a series of regularly timed ejections, presumably due to depletion of the readily-releasable neuronal Glut stores, recovering slightly after a 25 min recovery period without any stimulation.

Preliminary tests of the biocompatibility of these flexible neural probes during chronic implantation were performed using GFAP as a marker of astrocytes post-mortem. Rats were implanted bilaterally in the striatum with a flexible probe on one side and a silicon probe with similar dimensions on the contralateral side, and the animals were permitted to recover from anesthesia. In the example shown in Supplementary Fig. S9, 4 weeks after implantation, the soft probe demonstrated reduced astrocytic encapsulation compared to the stiff silicon probe, similar to reports of other flexible probes (Du et al., 2017; Nguyen et al., 2014). An example of data at 9 weeks is presented in Supplementary Fig. S10 showing an overall reduced level of GFAP expression surrounding the probes relative to the example shown at 4 weeks, with a thinner scar formation surrounding the ULTS probes compared to the silicon probes. The ULTS probes exhibits higher GFAP expression at the surface, which is possibly due to the hydrophobic nature of PDMS. Further improvement in the biocompatibility of ULTS probes for long-term applications may be achieved using anti-fouling coatings, such as poly(ethylene glycol) (PEG)-based materials, poly-L-lysine or hyaluronic acid (Zhang and Chiao, 2015; Zhou et al., 2010) or by the delivery of bioactive agents (Lecomte et al., 2017) to counter the hydrophobic nature of PDMS (Zhang and Chiao, 2015; Zhou et al., 2010).

4. Conclusion

The development of flexible neural probes is a promising approach

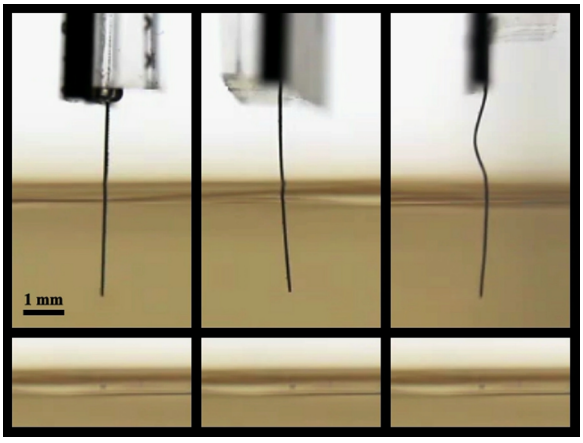

Movie 1. Comparison of Si (left), SU-8 (middle) and ULTS (right) probes with lateral and vertical movements in a brain phantom to simulate the micromotion between the probe and the brain. The implanted portion of ULTS probe remains steady relative to the brain phantom, while other probes created large "wounds" due to the relative motion. A video clip is available online. Supplementary material related to this article can be found online at doi:10.1016/j.bios.2019.01.060.

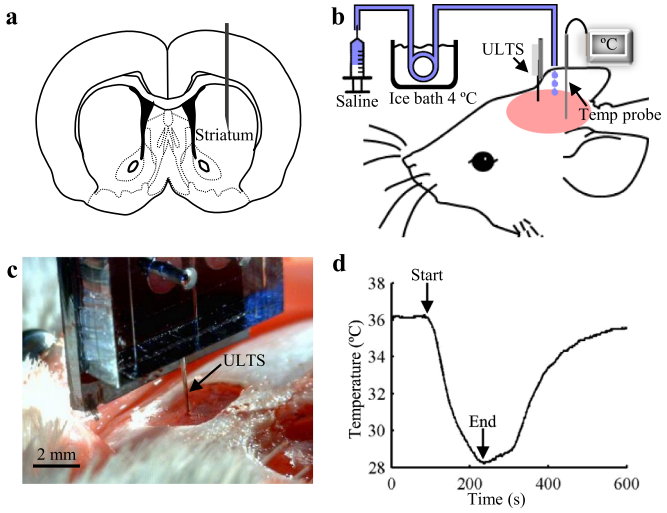

Fig. 5. Probe Implantation in Rats. (**a**) Schematic of a coronal brain slice illustrating the targeted implantation location in the rat striatum. (**b**) Schematic of the implantation procedure. Bilateral craniotomies were performed above the striata and chilled sterile saline was perfused across the skull surface. A miniaturized temperature probe was inserted remote from the recording site at the targeted implantation depth. (**c**) Optical image of a ULTS probe (arrow) implanted in a rat brain. (**d**) A representative brain temperature curve showing the brain cooling and temperature recovery process. Arrows indicate the start and end of the application of chilled saline solution.

to reduce immunoinflammatory response and improve the functionality for long-term applications. However, by reducing the dimensions aggressively, in order to achieve the desired flexibility, such probes often face challenges in the implantation process and the integration of multiple functionalities. In this paper, we designed, fabricated and validated the first ultra-soft, multifunctional neural probe that can be implanted deep into brain tissue without external shuttle carriers or coatings, which was made possible by using a liquid metal, Ga, and soft elastomer substrate in its construction. Taking advantage of the solid-to-liquid phase change of the metal at body temperature and the probe shape deformation, a tunable stiffness of 5 orders of magnitude was achieved. Probes were successively implanted 2 cm-deep into agarose gel "brain phantoms" and rat brain under cooled conditions, while they

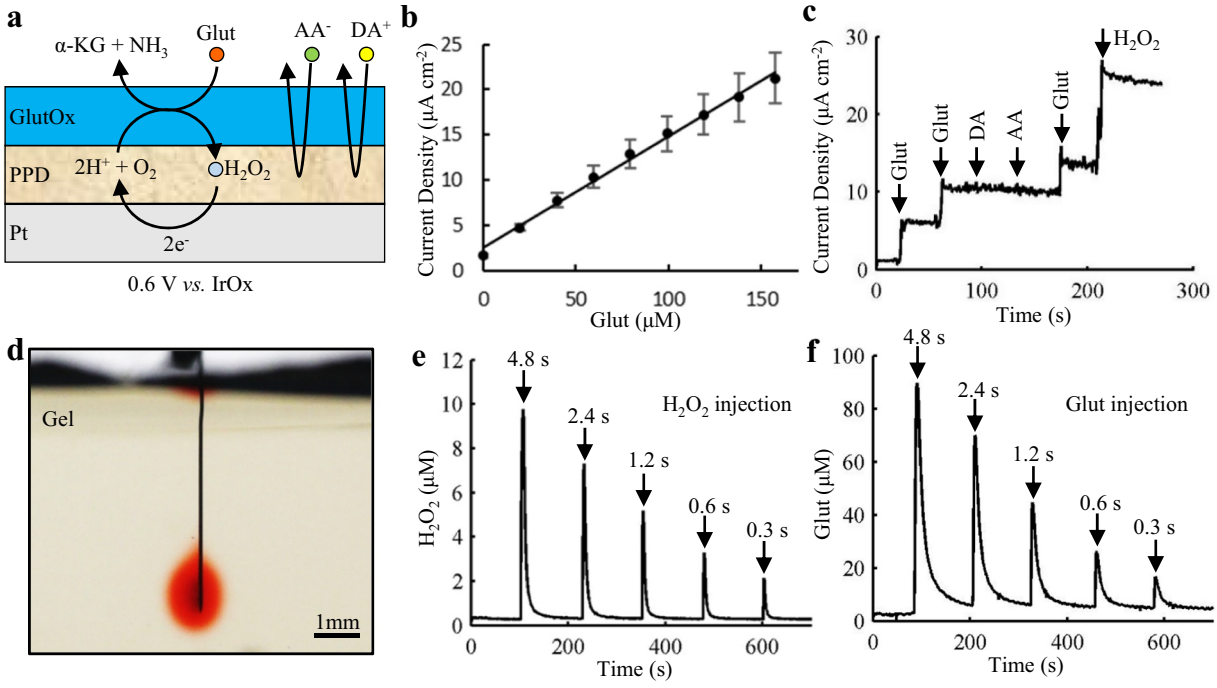

Fig. 4. *In vitro* characterization of biosensor and chemical delivery functions. (**a**) Schematic diagram of the coatings on a single electrode on the ULTS probe. (**b**) Calibration curve for Glut sensing showing a linear correlation in the physiological range, up to 160 μM. Mean ± SEM of 4 sensors. (**c**) Current response of a Glut biosensor to Glut, the physiological interferents – dopamine (DA) and ascorbic acid (AA), and H_2O_2 in stirred PBS solution (pH 7.4). Arrows indicate the sequential injections to give total concentrations of 20 μM Glut, 40 μM Glut, 5 μM DA, 250 μM AA, 60 μM Glut and 20 μM H_2O_2. (**d**) Optical image showing delivery of liquid (aqueous solution of Allura Red AC) into a brain phantom (0.6% agarose gel). (**e, f**) *In vitro* testing of chemical delivery in brain phantoms (0.6% agarose gel in aCSF). H_2O_2 (40 μM) (**e**) and Glut (150 μM) (**f**) were injected at 60 psi with injection duration of 4.8 s, 2.4 s, 1.2 s, 0.6 s and 0.3 s indicated by the arrows (injection volumes in the range ~1–20 nL).

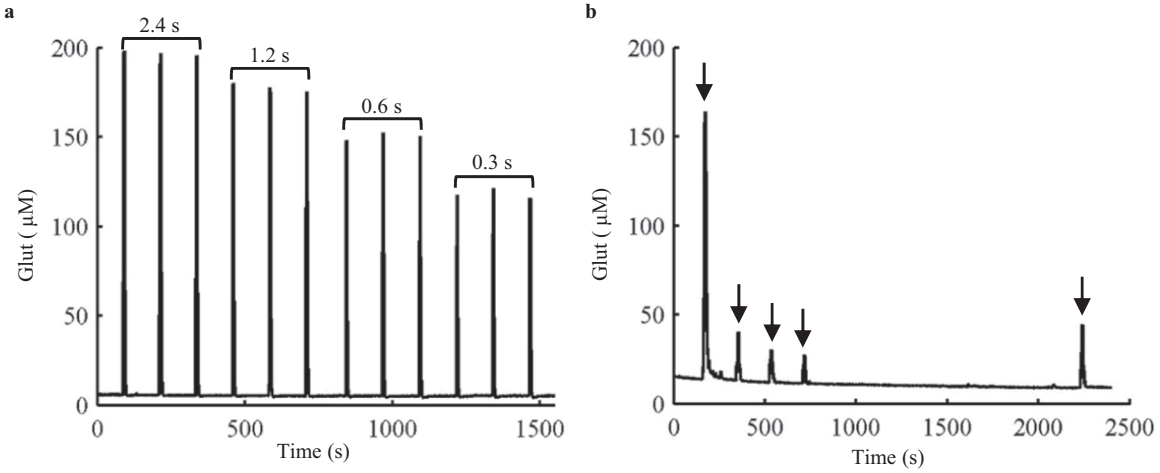

Fig. 6. *In vivo* characterization of biosensor and chemical delivery functions. (**a**) Detection of repeated injections of Glut (500 μM) *via* the fluid channel into the rat striatum. Glut solutions were injected at 2 min intervals at 60 psi with injection durations of 2.4 s, 1.2 s, 0.6 s and 0.3 s, respectively, indicated by the brackets. (**b**) Repeated injection (arrows) of potassium-enriched artificial cerebrospinal fluid (100 mM K+ aCSF) in rat striatum to induce Glut release. Solutions were injected at 60 psi with an injection duration of 4.8 s at 2 min intervals. Signal amplitude was considerably reduced following the initial stimulation, recovering only partially after a prolonged period (25 min) free from stimulation.

became ultra soft and flexible upon Ga melting at physiological temperature. With liquid metal wires, Pt electrodes and appropriate coatings, high-performance and stable electrochemical Glut sensing was demonstrated in both stiff and soft states with a sensitivity of 8.2 ± 1.2 pA/μM, detection limit of 0.39 ± 0.07 μM and response time of ~1 s, which are equivalent to the state-of-the-art silicon-based systems. *In vivo* chemical stimulation of Glut was demonstrated by injection of potassium-enriched aCSF through the integrated microfluidic channel. These PDMS-based microprobes of ultra-large tunable stiffness (ULTS), with potential for incorporation of functions such as optogenetics and electrophysiological recording, serve as an attractive platform for multifunctional chronic neural implants.

CRediT authorship contribution statement

Ximiao Wen: Conceptualization, Investigation, Formal analysis, Writing - review & editing. **Bo Wang:** Conceptualization, Investigation, Formal analysis, Writing - review & editing. **Shan Huang:** Investigation, Formal analysis, Writing - review & editing. **Tingyi "Leo" Liu:** Investigation, Formal analysis, Writing - review & editing. **Meng-Shiue Lee:** Investigation, Formal analysis, Writing - review & editing. **Pei-Shan Chung:** Investigation, Formal analysis, Writing - review & editing. **Yu Ting Chow:** Investigation, Formal analysis, Writing - review & editing. **I-Wen Huang:** Investigation, Formal analysis, Writing - review & editing. **Harold G. Monbouquette:** Supervision, Writing - review & editing. **Nigel T. Maidment:** Supervision, Conceptualization, Writing - review & editing. **Pei-Yu Chiou:** Supervision, Conceptualization, Writing - review & editing.

Acknowledgements

This work was supported by NIH Grant R01NS087494. We thank the Cui Lab for sharing the I.N.T.E.N.S.I.T.Y. MATLAB script on their website. All microfabrication steps were completed using equipment provided by the UCLA Nanoelectronics Research Facility.

Competing interests

The authors declare that they have no competing interests.

Appendix A. Supplementary material

Supplementary data associated with this article can be found in the online version at doi:10.1016/j.bios.2019.01.060.

References

Boehler, C., Stieglitz, T., Asplund, M., 2015. Biomaterials 67, 346–353.
Bruus, H., 2011. Lab Chip 11, 3742–3751.
Capadona, J.R., Tyler, D.J., Zorman, C.A., Rowan, S.J., Weder, C., 2012. MRS Bull. 37, 581–589.
Chen, J., Wise, K.D., Hetke, J.F., Bledsoe, S.C., 1997. IEEE Trans. Biomed. Eng. 44, 760–769.
Chow, Y.T., Man, T., Acosta-Vélez, G.F., Zhu, X., Wen, X., Chung, P.-S., Liu, T."Leo", Wu, B.M., Chiou, P.-Y., 2018. Adv. Sci. 5, 1700711.
Danbolt, N.C., 2001. Progress. Neurobiol. 65, 1–105.
Dickey, M.D., 2017. Adv. Mater. 29, 1.
Dietrich, W.D., Atkins, C.M., Bramlett, H.M., 2009. J. Neurotrauma 26, 301–312.
Du, Z.J., Kolarcik, C.L., Kozai, T.D.Y., Luebben, S.D., Sapp, S.A., Zheng, X.S., Nabity, J.A., Cui, X.T., 2017. Acta Biomater. 53, 46–58.
Eriksson, E., Engberg, G., Bing, O., Nissbrandt, H., 1999. Neuropsychopharmacology 20, 287–296.
Felix, S.H., Shah, K.G., Tolosa, V.M., Sheth, H.J., Tooker, A.C., Delima, T.L., Jadhav, S.P., Frank, L.M., Pannu, S.S., 2013. J. Vis. Exp.
Galuske, R.A.W., Schmidt, K.E., Goebel, R., Lomber, S.G., Payne, B.R., 2002. PNAS 99, 17083–17088.
Gass, J.T., Foster Olive, M., 2008. Biochem Pharmacol. 75, 218–265.
Girard, P., Bullier, J., 1989. J. Neurophysiol. 62, 1287–1302.
Hallfors, N., Khan, A., Dickey, M.D., Taylor, A.M., 2013. Lab Chip 13, 522–526.
Jeong, J.-W., McCall, J.G., Shin, G., Zhang, Y., Al-Hasani, R., Kim, M., Li, S., Sim, J.Y., Jang, K.-I., Shi, Y., Hong, D.Y., Liu, Y., Schmitz, G.P., Xia, L., He, Z., Gamble, P., Ray, W.Z., Huang, Y., Bruchas, M.R., Rogers, J.A., 2015a. Cell 162, 662–674.
Jeong, J.-W., Shin, G., Park, S.I., Yu, K.J., Xu, L., Rogers, J.A., 2015b. Neuron 86, 175–186.
Jorfi, M., Skousen, J.L., Weder, C., Capadona, J.R., 2015. J. Neural Eng. 12, 011001.
Kim, T., McCall, J.G., Jung, Y.H., Huang, X., Siuda, E.R., Li, Y., Song, J., Song, Y.M., Pao, H.A., Kim, R.-H., Lu, C., Lee, S.D., Song, I.-S., Shin, G., Al-Hasani, R., Kim, S., Tan, M.P., Huang, Y., Omenetto, F.G., Rogers, J.A., Bruchas, M.R., 2013. Science 340, 211–216.
Kuluz, J.W., Gregory, G.A., Yu, A.C., Chang, Y., 1992. Stroke 23, 1792–1796.
Lecomte, A., Descamps, E., Bergaud, C., 2017. J. Neural Eng.
Lee, J.H., Kim, H., Kim, J.H., Lee, S.-H., 2016. Lab Chip 16, 959–976.
Liu, J., Fu, T.-M., Cheng, Z., Hong, G., Zhou, T., Jin, L., Duvvuri, M., Jiang, Z., Kruskal, P., Xie, C., Suo, Z., Fang, Y., Lieber, C.M., 2015. Nat. Nanotechnol. 10, 629–636.
Long, M.A., Fee, M.S., 2008. Nature 456, 189–194.
Luan, L., Wei, X., Zhao, Z., Siegel, J.J., Potnis, O., Tuppen, C.A., Lin, S., Kazmi, S., Fowler, R.A., Holloway, S., Dunn, A.K., Chitwood, R.A., Xie, C., 2017. Sci. Adv. 3, e1601966.
McAllister, D.V., Wang, P.M., Davis, S.P., Park, J.-H., Canatella, P.J., Allen, M.G., Prausnitz, M.R., 2003. PNAS 100, 13755–13760.
Minev, I.R., Musienko, P., Hirsch, A., Barraud, Q., Wenger, N., Moraud, E.M., Gandar, J., Capogrosso, M., Milekovic, T., Asboth, L., Torres, R.F., Vachicouras, N., Liu, Q., Pavlova, N., Duis, S., Larmagnac, A., Vörös, J., Micera, S., Suo, Z., Courtine, G., Lacour, S.P., 2015. Science 347, 159–163.

Nguyen, J.K., Park, D.J., Skousen, J.L., Hess-Dunning, A.E., Tyler, D.J., Rowan, S.J., Weder, C., Capadona, J.R., 2014. J. Neural Eng. 11, 056014.
Oku, T., Fujii, M., Tanaka, N., Imoto, H., Uchiyama, J., Oka, F., Kunitsugu, I., Fujioka, H., Nomura, S., Kajiwara, K., Fujisawa, H., Kato, S., Saito, T., Suzuki, M., 2009. J. Neurosurg. 110, 1209–1217.
Park, S.I., Shin, G., McCall, J.G., Al-Hasani, R., Norris, A., Xia, L., Brenner, D.S., Noh, K.N., Bang, S.Y., Bhatti, D.L., 2016. Proc. Natl. Acad. Sci. USA 113, E8169–E8177.
Peel, T.R., Dash, S., Lomber, S.G., Corneil, B.D., 2017. J. Neurosci. 37, 11715–11730.
Percy, A., Widman, S., Rizzo, J.A., Tranquilli, M., Elefteriades, J.A., 2009. Ann. Thorac. Surg. 87, 117–123.
Reed, M.L., Lye, W.-K., 2004. Proc. IEEE 92, 56–75.
Rivnay, J., Wang, H., Fenno, L., Deisseroth, K., Malliaras, G.G., 2017. Sci. Adv. 3, e1601649.
Rohatgi, P., Langhals, N.B., Kipke, D.R., Patil, P.G., 2009. Neurosurg. Focus 27, E8.
Sim, J.Y., Haney, M.P., Park, S.I., McCall, J.G., Jeong, J.-W., 2017. Lab Chip 17, 1406–1435.
Spector, R., 1977. New Engl. J. Med. 296, 1393–1398.
Subbaroyan, J., Martin, D.C., Kipke, D.R., 2005. J. Neural Eng. 2, 103–113.
Tien, L.W., Wu, F., Tang-Schomer, M.D., Yoon, E., Omenetto, F.G., Kaplan, D.L., 2013. Adv. Funct. Mater. 23, 3185–3193.
Tolosa, V.M., Wassum, K.M., Maidment, N.T., Monbouquette, H.G., 2013. Biosens. Bioelectron. 42, 256–260.
Wahono, N., Qin, S., Oomen, P., Cremers, T.I.F., de Vries, M.G., Westerink, B.H.C., 2012. Biosens. Bioelectron. 33, 260–266.
Walker, E., Wang, J., Hamdi, N., Monbouquette, H.G., Maidment, N.T., 2007. Analyst 132, 1107.
Wang, B., Koo, B., Huang, L., Monbouquette, H.G., 2018. Analyst 143, 5008–5013.
Wang, H., Wang, B., Normoyle, K.P., Jackson, K., Spitler, K., Sharrock, M.F., Miller, C.M., Best, C., Llano, D., Du, R., 2014. Front. Neurosci. 8.
Ware, T., Simon, D., Liu, C., Musa, T., Vasudevan, S., Sloan, A., Keefer, E.W., Rennaker, R.L., Voit, W., 2014. J. Biomed. Mater. Res. Part B: Appl. Biomater. 102, 1–11.
Wassum, K., Tolosa, V., Tseng, T., Balleine, B., Monbouquette, H., Maidment, N., 2012. J. Neurosci. 32, 2734–2746.
Wassum, K.M., Tolosa, V.M., Wang, J., Walker, E., Monbouquette, H.G., Maidment, N.T., 2008. Sensors 8, 5023–5036.
Weltman, A., Yoo, J., Meng, E., 2016. Micromachines 7, 180.
Wu, F., Tien, L.W., Chen, F., Berke, J.D., Kaplan, D.L., Yoon, E., 2015. J. Microelectromech. Syst. 24, 62–69.
Xiang, Z., Yen, S.-C., Xue, N., Sun, T., Tsang, W.M., Zhang, S., Liao, L.-D., Thakor, N.V., Lee, C., 2014. J. Micromech. Microeng. 24, 065015.
Zhang, H., Chiao, M., 2015. J. Med Biol. Eng. 35, 143–155.
Zhou, J., Ellis, A.V., Voelcker, N.H., 2010. Electrophoresis 31, 2–16.